Modeling of Casting, Welding and Advanced Solidification Processes X
Edited by D.M. Stefanescu, J. Warren, M. Jolly and M. Krane
TMS (The Minerals, Metals & Materials Society), 2003

GRAIN EVOLUTION AND MACROSEGREGATION IN AN AL-4.0%CU CASTING: SIMULATION AND EXPERIMENTAL EVALUATION

M. Wu, A. Ludwig, P. R. Sahm and A. Bührig-Polaczek

Foundry Institute, Aachen University, Intzestr. 5, D-52072 Aachen, Germany

Abstract

A two phase volume averaging approach was used to model the solidification of an Al-4.0wt.%Cu plate casting, including nucleation, grain structure and macrosegregation formation under the influence of melt convection and grain sedimentation. With Ti as grain refiner the solidification morphology of this alloys was simplified as globular equiaxed. Both the liquid and solid phases were modeled as two separated and interpenetrating continua. The conservation equations for mass, momentum, species and enthalpy for both phases, and an additional grain density conservation equation were solved. Interactions between the melt and the solid such as mass transfer, friction and drag, solute partitioning and release of latent heat as well as nucleation were included in corresponding exchange and source terms. Evaluation efforts were made by comparing the numerical predictions with experimental findings. The numerically precicted grain size distribution in a plate casting (Al-4wt%Cu) was found to agree reasonably with the metallographic analyses.

Introduction

Prediction of grain distribution and macrosegregation such as in ingot or continuous casting is of special interest to the material processing industry. In order to understand the grain evolution and the outcome of macrosegregations during solidification, following processes must be taken into account: nucleation, grain growth, heat and mass transfer, melt convection, grain movement, solute partitioning and transport, etc. Numerical methods to study this problem have only been developed in recent years, when all the conservation equations for multiphase problem could be coupled and solved simultaneously[1-2]. As most promising model the volume-averaging approach developed by Beckermann's group[2-8] was presented. For globular equiaxed solidificaton this approach was further modified by Ludwig et al[9-11], who avoided some uncertainties which appeared in the pioneering model[12-13]. This modified model was applied to study the solidification in industrial alloy Al-4wt%Cu. With Ti as grain refiner this alloy is known to solidify with a near globular equiaxed morphology.

Numerical model

The two phase volume averaging model for globular equiaxed solidification was described previously[9-11]. The conservation equations, source terms, exchange terms and some auxiliary terms are shown in Table I.

Table I. Conservation equations, source and exchange terms and auxiliary equations for the numerical model of globular equiaxed solidification

Conservation equations

Mass:

$$\frac{\partial}{\partial t}(f_l\rho_l)+\nabla\cdot(f_l\rho_l\vec{u}_l)=M_{ll}$$

$$\frac{\partial}{\partial t}(f_e\rho_e)+\nabla\cdot(f_e\rho_e\vec{u}_e)=M_{el}$$

Momentum:

$$\frac{\partial}{\partial t}(f_l\rho_l\vec{u}_l)+\nabla\cdot(f_l\rho_l\vec{u}_l\otimes\vec{u}_l)=-f_l\nabla p+\nabla\cdot\bar{\bar{\tau}}_l+f_l\rho_l\vec{g}+\vec{U}_{ll}$$

$$\frac{\partial}{\partial t}(f_e\rho_e\vec{u}_e)+\nabla\cdot(f_e\rho_e\vec{u}_e\otimes\vec{u}_e)=-f_e\nabla p+\nabla\cdot\bar{\bar{\tau}}_e+f_e\rho_e\vec{g}+\vec{U}_{el}$$

where $\bar{\bar{\tau}}_l=\mu_l f_l\left(\nabla\cdot\vec{u}_l+(\nabla\cdot\vec{u}_l)^T\right)$ and $\bar{\bar{\tau}}_e=\mu_e f_e\left(\nabla\cdot\vec{u}_e+(\nabla\cdot\vec{u}_e)^T\right)$

Species:

$$\frac{\partial}{\partial t}(f_l\rho_l c_l)+\nabla\cdot(f_l\rho_l\vec{u}_l c_l)=\nabla\cdot(f_l\rho_l D_l\nabla c_l)+C_{cl}$$

$$\frac{\partial}{\partial t}(f_e\rho_e c_e)+\nabla\cdot(f_e\rho_e\vec{u}_e c_e)=\nabla\cdot(f_e\rho_e D_e\nabla c_e)+C_{ce}$$

Enthalpy:

$$\frac{\partial}{\partial t}(f_l\rho_l h_l)-\nabla\cdot(f_l\rho_l\vec{u}_l h_l)=\nabla\cdot(f_l k_l\nabla\cdot T_l)+Q_{il}$$

$$\frac{\partial}{\partial t}(f_e\rho_e h_e)+\nabla\cdot(f_e\rho_e\vec{u}_e h_e)=\nabla\cdot(f_e k_e\nabla\cdot T_e)+Q_{ie}$$

where $h_l=\int_{T_{ref}}^{T_l}c_{p(l)}dT+h_l^{ref}$ and $h_e=\int_{T_{ref}}^{T_e}c_{p(e)}dT+h_e^{ref}$

Grain transport.

$$\frac{\partial}{\partial t}n+\nabla\cdot(\vec{u}_e n)=N$$

Source terms:

Nucleation:

$$N=\frac{d\Delta T}{dt}\cdot\frac{n_{max}}{\sqrt{2\pi}\cdot\Delta T_\sigma}\cdot e^{-\frac{1}{2}\left[\frac{\Delta T-\Delta T_n}{\Delta T_\sigma}\right]^2}$$

Exchange terms

Mass transfer

$$M_{ls} = \xi_{ls} \cdot \Delta c \cdot (n \cdot \pi d_s^3) \cdot \rho_s \cdot f_s \tag{7}$$

Momentum:

$$\vec{U}_{ls} = \vec{U}_{ls}^{d} + \vec{U}_{ls}^{p} \qquad \vec{U}_{ls}^{p} = \vec{u}^{*} \cdot M_{ls} \qquad \vec{U}_{ls}^{d} = K_{ls}(\vec{u}_l - \vec{u}_s) \tag{8}$$

Species:

$$C_{ls} = C_{ls}^{d} + C_{ls}^{p} \qquad C_{ls}^{p} = c^{*} \cdot M_{ls} \qquad C_{ls}^{d} \text{ neglected} \tag{9}$$

Enthalpy:

$$Q_{ls} = Q_{ls}^{d} + Q_{ls}^{p} \qquad Q_{ls}^{p} = h^{*} \cdot M_{ls} \qquad Q_{ls}^{d} = H^{*} \cdot (T_l - T_s) \tag{10}$$

Auxiliary terms

Mix concentration:

$$c_{mix} = \frac{c_l \cdot \rho_l \cdot f_l + c_s \cdot \rho_s \cdot f_s}{\rho_l \cdot f_l + \rho_s \cdot f_s} \tag{11}$$

Grain diameter:

$$d_s = \left(6 \cdot f_s / \pi \cdot n\right)^{\frac{1}{3}} \tag{12}$$

Solid viscosity:

$$\mu_s = \begin{cases} \dfrac{\mu_l}{f_s} \cdot \left| \left(1 - f_s / f_s^{*}\right)^{-2.5 f_s^{*}} - \left(1 - f_s\right) \right| & \text{when } f_s < f_s^{*} \\ \infty & \text{else} \end{cases} \tag{13}$$

The liquid and solid phases are transported according to the mass conservation Eq.(1), taking solidification (remelting) into account through a mass transfer term $M_{ls}\,(=M_{sl})$, which is defined in Eq.(7). The volume fractions of both phases are subject to $f_l + f_s = 1$. Momentum exchange $\vec{U}_{ls}\,(=-\vec{U}_{sl})$ in Eq.(2) consists of two parts: one due to mass transfer $\vec{U}_{ls}^{p}$ and the other due to drag force $\vec{U}_{ls}^{d}$. Details about the drag force model are given elsewhere[9, 14-15]. A solid viscosity μ_s is empirically defined in Eq.(13) based on a mixing rule[3-6].

The solute concentration in the liquid and solid are calculated by solving Eq.(3). The solute partitioning at the liquid-solid interface due to phase change C_{ls}^{p} is taken into account[9], while the solute diffusional exchange at the liquid-solid interface C_{ls}^{d} is neglected. A mix concentration c_{mix} is defined in Eq.(11) to describe the macrosegregation.

The enthalpy conservation Eq.(4) for both phases are also solved separately, hence we get two different temperatures T_l and T_s. With a relatively large diffusional heat exchange term Q_{ls}^{d} between the liquid and solid phases, the temperature difference can be leveled out, and an thermal equilibrium ($T_l \approx T_s$) is obtained. The enthalpy difference ($h_l - h_s = \Delta h_f$) defines the latent heat. Details to handle the latent heat in this model is described previously[9].

An additional conservation Eq.(5) is solved to obtain the grain density distribution n. The grains are transported according to $\vec{u}_s$. An empirical 3-parameter nucleation law (Eq.(6)) is used[1]. With the known n and f_s, the averaged grain size d_s is estimated by Eq.(12).

Problem description and experimental evaluation procedure

Due to the limitation of the computer capacity, the two phase solidification simulation is made in a 2D section of the plate casting. The configuration of the section is shown in Fig. 1. The mold filling simulation by a commercial software MAGMASOFT® is referred to determine the initial temperature distribution for the solidification simulation. The mold (steel die) is

considered here as conducting wall with initial temperature of 573 K. The casting/mold heat exchange coefficient $H_{c\text{-}m}$ is taken to be 800 W/(m^{2}K). The heat exchange coefficient between the mold and the environment $H_{m\text{-}a}$ is 30 W/(m^{2}K). Also a convection boundary condition at the casting top is assumed, and $H_{c\text{-}a}$ is 50 W/(m^{2}K). A non-slip boundary condition is applied for liquid phase at the melt/mold interface, while the solid phase which nucleate on the mold wall can move freely. The calculation domain is meshed into square volume elements with mesh size of 2x2 mm^2. The time step as small as $\Delta t = 2 \times 10^{-4}$ s is used in the simulation. A single run of the simulation takes 7~10 days on a SGI Octane workstation (R12000).

Table II shows the physical properties of both casting and mold and the phase diagram parameters of the cast alloy (Al-4wt.% Cu). Different densities of liquid ρ_l and solid ρ_s are only considered in momentum conservation equations, where the Boussinesq approach is used to model the sedimentation of the solid phase during solidification. The ρ_l and ρ_s are considered elsewhere equal and constant (2606 kg/m^3), hence the solidification shrinkage and thermosolutal convection are ignored. The parameters for the nucleation law[1] in Eq.(6) are $n_{max} = 1.5 \cdot 10^{12}$ m^{-3}, $\Delta T_N = 20$ K, $\Delta T_\sigma = 8$ K.

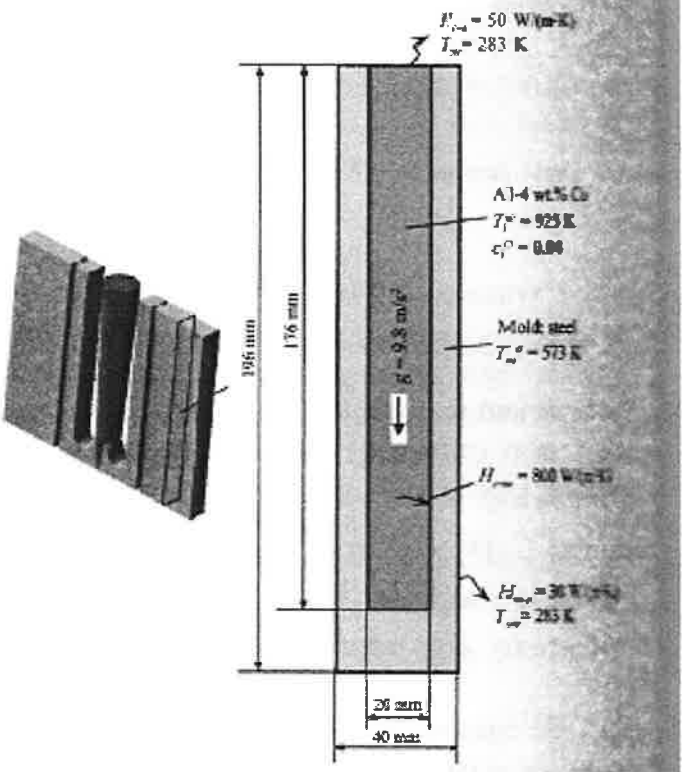

Figure 1: Configuration of the studied case.

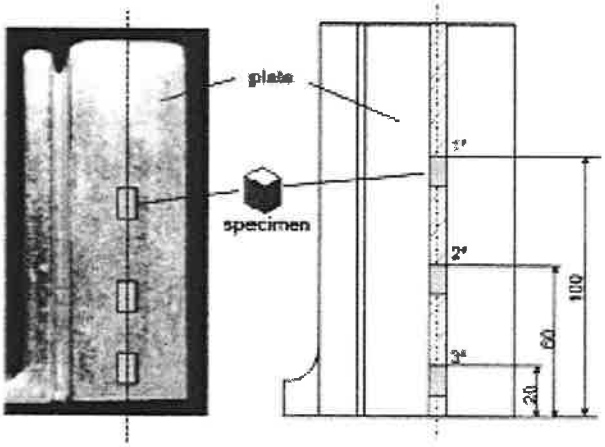

a) Specimen positions.

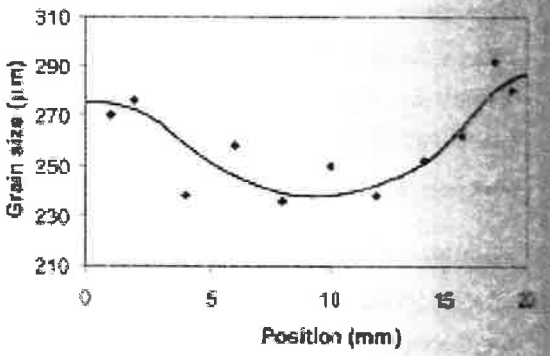

c) Measured grain size distribution (2a)

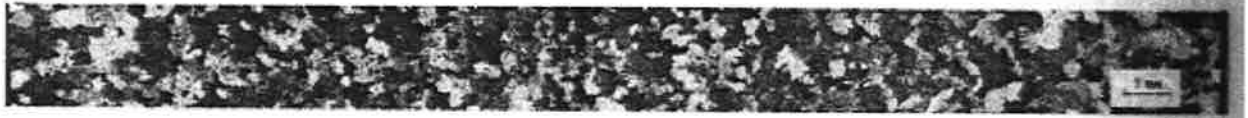

b) Typical metallograph across the thickness direction of the plate (position 2a)

Figure 2: Metallographical study of the grain size distribution in the real plate casting

Table II. Thermophysical and thermodynamic properties used in the simulation

$\rho_l = 2606\ kg/m^3$	$c_{p(s)} = 766\ J/kg/K$	$D_l^{Cu} = 8 \times 10^{-13}\ m^2/s$
$\rho_s = 2743\ kg/m^3$	$\rho_{mold} = 7734\ kg/m^3$	$\mu_l = 1.2 \times 10^{-3}\ kg/m/s$
$k_l = 77\ W/m/K$	$k_{mold} = 40.35\ W/m/K$	$T_f = 933.5\ K$
$k_s = 153\ W/m/K$	$c_{p(mold)} = 621\ J/kg/K$	$k = 0.145$
$c_{p(l)} = 1179\ J/kg/K$	$D_s^{Cu} = 5 \times 10^{-9}\ m^2/s$	$m = -344\ K$

For evaluation the real casting was poured. As shown in Fig.2 (a), the casting was sectioned, and specimens were taken at different positions. With Baker etching the microscopic metallographic examination across the thickness direction was made, Fig.2 (b). The grain size was measured manually in equal interval (2mm) across the section. Around each measuring point 10 random grains were selected, and the grain size was averaged. In this way the grain size distribution, Fig. 2 (c), was obtained. In addition to the grain size distribution the macrosegregation was also analyzed with EDX (energy dispersive X-ray) method.

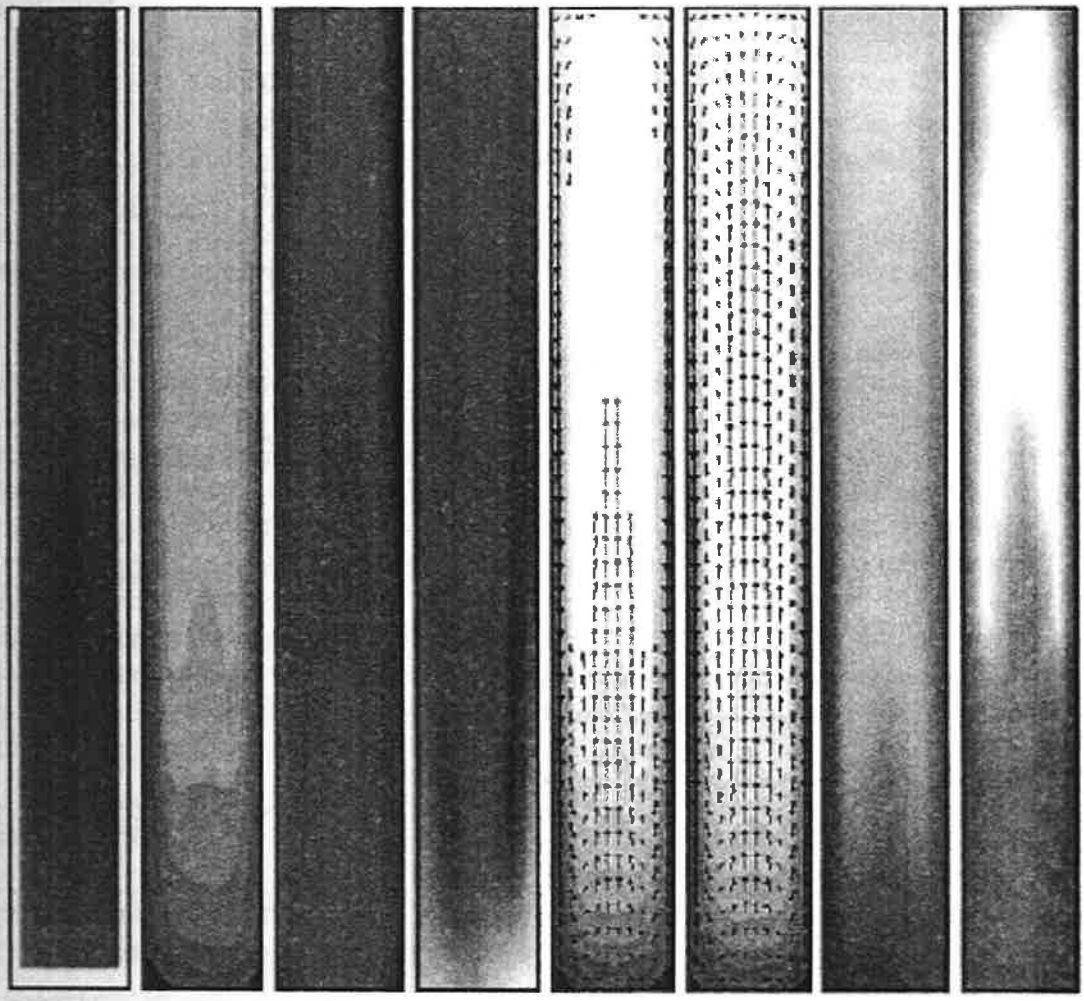

Figure 3: Simulation result 7 s after start of cooling. The arrows of both velocity fields are continuously scaled starting from zero to the maximum value. All other quantities are scaled equidistantly by 30 gray levels, with light representing the lowest and dark the highest value. T: 900~919 K, c_l: 0.04~0.2, $M_{\bar{u}}$: -1.7~227 kg/m^3/s, c_{mix}: 0.037~0.042, f_s: 0~1, $\bar{u}_l$: 0~21 mm/s, $\bar{u}_s$: 0~20 mm/s, n: 0~130 mm^{-3}, d_s: 0~0.37 mm.

Results and discussions

A typical simulation result at 7 s is shown in Fig. 3. As soon as T drops below the liquidus along the mould walls, nucleation and solidification start. Due to gravity grains nucleated near the vertical walls sink downwards. Sinking of the grains leads to the accumulation of solid phase in the bottom region. As the local fraction solid f_s exceeds the packing limit (0.637), the grains settle there and the velocity of the solid $\vec{u}_s$ vanishes. Sedimentation occurs. As the solid and liquid are coupled through the momentum exchange terms, the melt is drawn by sinking solid. Two vortices form in the bulk melt - one clockwise in the right half and the anticlockwise in the left haft of the casting. The flow currents are so strong that part of the grains in bottom region are brought up to the upper region again. As shown in Fig. 3, special distributions of fraction solid f_s, solid velocity $\vec{u}_s$, grain density n and average grain size s are develcped.

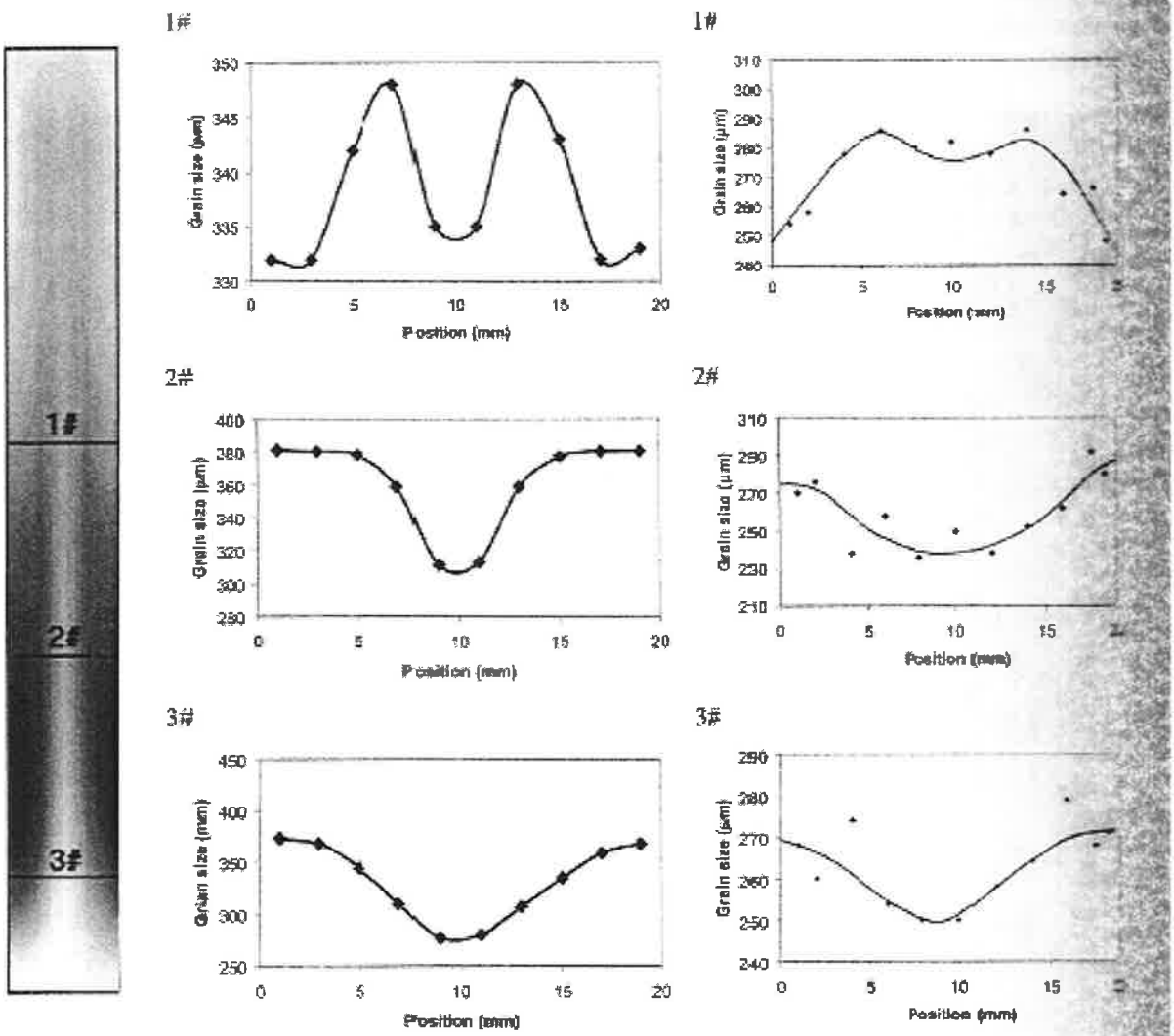

a) simulated grain size distribution.

b) Simulated grain size distribu-tion across the casting section at 3 different positions 1#, 2# and 3#.

c) The experimentally measured grain size distribution at the corresponding positions 1#, 2# and 3#.

Figure 4: Comparison of the numerically predicted grain size distribution to the experimentally measured results. The grain size distribution of the whole section is shown with 3 gray levels, with light showing the smallest grains (262 μm), and dark the largest (390 μm).

The final grain size distribution is shown in Fig. 4 (a). In the lower bottom region fine grains (high grain density n and small grain size d_s) are predicted. There are two reasons for these fine grains: one is the initial high cooling rate, the other is the sedimentation. The initially nucleated fine grains in lower regions sink and settle at the bottom. As shown by the simulation results the flow currents bring also some grains from bottom regions to the casting center. The temperature in the casting center is higher, and the solidification rate (mass transfer rate M_s) is lower than the surface regions. Therefore the grain growth in the casting center is much slower than in casting surface regions. Even remelting occurs occasionally. Both the grain migration and the lower growth rate are responsible for the small grains in the casting center. The largest grains (~390 μm) locate near the casting surface and about 30 mm above the casting bottom. The formation of these large grain zones are explained as following. Grains nucleated in upper regions sink along the vertical walls. They grow while sinking. As they reach the lower regions and settle there they grow to the maximum size.

The numerically predicted and the experimentally measured grain size distributions are directly compared in Fig. 4 (b-c). At the position 2# and 3#, both numerical simulation and experimental results show relative large grains near the surface regions and fine grains in the casting central region. At the position 1#, a 'M'-shape distribution is observed and predicted. From this comparison, the grain size distribution of the real casting agrees qualitatively well with the numerical prediction. However, the absolute values for the grain sizes are somehow different. They are numerically predicted to be 262~390 μm, while the experimentally measured are 230~300 μm. The reasons for this difference are manifold, e.g. simplifying modeling assumptions, uncertain thermal physical properties, accuracy of the numerical calculation, mesh quality and uncertainty of the nucleation parameters. Especially the nucleation parameters have a high impact on the final grain size predicted by the numerical model.

Macrosegregations are quantitatively described by the mix concentration c_{mix}. The development of macrosegregations are a direct outcome from the grain sedimentation and the melt convection. The grains which reveal a low alloy content compared to the melt sink downwards, accumulate and settle in the bottom regions. According to the c_{mix} definition, Eq.(11), the regions with high grain settlement rate have always negative segregation. On the other hand, the flow current carries the solute enriched melt upwards, so that a positive segregation occurs in the upper regions. To verify this prediction the real casting was EDX analyzed. The experimental macrosegregation measurements are relatively scatter. It is difficult to compare the experimental data to the numerical results quantitatively. However, both the numerical simulation and the measured results show the same tendency: negative macrosegregation in the lower regions and positive macrosegregation in the upper regions.

Closing remarks

This paper compares the two phase modeling results with experimental findings gained on a plate casting. In consideration of the model simplifications and some difficulties, which still need further developments, we find the agreement between the simulation and the experiment encouraging. It implies (or indicates) that

- the recent model can aid to study the solidification fundamentals including nucleation and grain evolution in the presence of melt convection and grain sedimentation;
- the above discussed mechanisms for the grain movement and macrosegregation formation in the plate casting are reasonable;
- the recent model can be further developed to predict and control macrostructure and macrosegregation.

Acknowledgement

This work was financially supported by the German Science Foundation (DFG) as part of the collaborative research centers "Integral Materials Modeling". The authors also acknowledge the excellent technical assistance of Dr. Pelzer and Dr. Braun with FLUENT Germany.

References

1. M. Rappaz, "Modeling of microstructure formation in solidification processes," Int. Mater. Rev., 34(1989), 93-123.
2. C. Beckermann, and R. Viskanta, "Mathematical modeling of transport phenomena during alloy solidification," Appl. Mech. Rev., 46(1993), 1-27.
3. J. Ni, and C. Beckermann, "A volume-averaged two-phase model for transport phenomena during solidification," Metall. Trans. B, 22B(1991), 349-361.
4. C.Y. Wang, and C. Beckermann, "Equiaxed dendritic solidification with convection: I. Multiscale/multiphase modeling," Metall. Mater. Trans. A, 27A(1996), 2754-2764.
5. C.Y. Wang, and C. Beckermann, "Equiaxed dendritic solidification with convection: II. Numerical simulations for an Al-4wt%Cu alloy," Metall. Mater. Trans. A, 27A(1996), 2765-2783.
6. C.Y. Wang, and C. Beckermann, "Equiaxed dendritic solidification with convection: III. Comparisons with NH_4Cl-H_2O experiments," Metall. Mater. Trans. A, 27A(1996), 2784-2795.
7. C. Beckermann, "Modeling segregation and grain structure development in equiaxed solidification with convection," JOM 49(1997), 13-17.
8. A.V. Reddy, and C. Beckermann, "Modeling of macrosegregation due to thermosolutal convection and contraction-driven flow in direct chill continuous casting of an Al-Cu round ingot," Metall. Mater. Trans. B, 28B(1997), 479-489.
9. A. Ludwig, and M. Wu, "Modeling of globular equiaxed solidification with a two phase approach," Accepted for publication in Metall. Mater. Trans. A (2002).
10. A. Ludwig, G. Ehlen, M. Pelzer, and P.R. Sahm, "Simulation of solid movement during solidification by a simple multiphase approach," in Proc. MCWASP IX, SIM2000, Aachen, Shaker-Verlag (2000), 175-182.
11. A. Ludwig, M. Wu, G. Ehlen, and P.R. Sahm, "Numerical description of solid movement during equiaxed solidification using a two-phase modeling approach," (Materials Week 2000, Munich, Germany, Sept. 25-28, 2000).
12. J. Ni, and F.P. Incropera, "Extension of the continuum model for transport phenomena occurring during metal alloy solidification: I. The conservation equations," Inter. J. Heat Mass Transfer, 38(1995), 1271-1284.
13. J. Ni, and F.P. Incropera, " Extension of the continuum model for transport phenomena occurring during metal alloy solidification: II. Microscopic considerations," Inter. J. Heat Mass Transfer, 38(1995), 1285-1296.
14. R.B. Bird, W.E. Stewart, and E.N. Lightfoot, Transport Phenomena, (New York, NY: John Wiley & Sons, 1960).
15. C.Y. Wang, S. Ahuja, C. Beckermann, and H.C. de Groh, "Multiparticle interfacial drag in equiaxed solidification," Metall. Mater. Trans. B, 26B(1995), 111-119.